[6]A. J. Dessler, F. C. Michel, H. E. Rorschach, and G. T. Trammell, Phys. Rev. 168, 737 (1968). See also J. T. Moore and D. Kuhlmann-Wilsdorf, Mater. Sci. Eng, 3, 183 (1968).
[7]M. Peshkin, Ann. Phys. (N.Y.) 16, 1 (1968).
[8]C. Herring, Phys. Rev. 171, 1361 (1968).
[9]M. Peshkin, Phys. Letters 29A, 181 (1969).
[10]J. W. Beams, Phys. Rev. Letters 21, 1093 (1968).
[11]M. V. Barnhill, Phys. Letters 27A, 461 (1968). For a discussion of rotating superconductors, see B. S. deWitt, Phys. Rev. Letters 16, 1092 (1966); G. Papini (unpublished).
[12]P. P. Craig, Phys. Rev. Letters 22, 700 (1969).
[13]W. A. Harrison, Phys. Rev. 180, 1606 (1969).
[14]D. M. Newns, Phys. Rev. (to be published).
[15]N. D. Lang, Solid State Commun. 7, 1047 (1969).
[16]P. Hohenberg and W. Kohn, Phys. Rev. 136, B864 (1964); W. Kohn and L. J. Sham, *ibid.* 140, A1133 (1965).
[17]P. Siemens [Phys. Rev. C 1, 98 (1970] has made extensive use of WKB solutions to expand on the work of Kohn and Sham (Ref. 16).
[18]L. I. Schiff, Proceedings of the Fifth International Conference on Gravitation and the Theory of Relativity, Tbilisi, USSR, 1968 (unpublished).

PHYSICAL REVIEW B VOLUME 1, NUMBER 12 15 JUNE 1970

Theory of Electronic Properties of Thin Films of *d*-Band Metals

Bernard R. Cooper and Alan J. Bennett
General Electric Research and Development Center, Schenectady, New York 12301
(Received 1 December 1969)

We have examined the changes in the nature of the *d*-band states in crystals of fcc transition and noble metals as the crystals become very thin. The calculated effects can be categorized as size effects and as surface effects. The size effects are the changes from states having a semicontinuous variation of energy with varying wave vector parallel to the small dimension to states having discrete energy values. These effects result from the loss of translational and cubic symmetry, and exist even when the overlap integrals are the same within the surface planes as within the interior planes of the crystal. The effects found are qualitatively different for single-crystal fcc films with ⟨100⟩ and ⟨111⟩ normals, respectively. Surface effects are changes in the electronic structure associated with changes of overlap integrals within the surface planes. We show how such changes lead to the existence of *d*-band surface states for a ⟨100⟩ film. For ⟨111⟩ films, there is an even more striking qualitative effect involving surface states. This is the appearance of surface states for one area of the two-dimensional Brillouin zone even when the overlap integrals within the boundary planes are the same as those within the interior planes of the film. We illustrate all these effects by calculations for the Γ_{12} bands (i.e., the bands corresponding to E-symmetry *d* atomic states), using realistic parameters for Ni with crystals 5 and 11 atomic layers thick. Finally, we discuss the prospects for experimental work – in particular, investigations of the density of states and of various anisotropic effects associated with the departure from cubic symmetry on going to a very thin film.

I. INTRODUCTION

In this paper, we examine the nature of the expected changes in the electronic structure associated with the *d* bands in fcc transition and noble metals on going to very thin crystals (i.e., single-crystal films). As one dimension of a crystal becomes very thin, we expect a change in the nature of the energy eigenstates corresponding to a change in the variation of energy with wave vector normal to the crystal surface from a semicontinuous band to discrete values. Also, depending on the surface conditions, surface states can appear, and the number of such states can be relatively much more important than for bulk solids. Going to a thin crystal also involves a fundamental change in the symmetry properties of a crystal. A very thin crystal of a cubic metal such as copper or nickel is no longer truly cubic, and this departure from cubic symmetry is reflected in the nature of the electronic states.

The above changes in electronic structure may have significant effects on various physical properties of a film which depend on the electronic density of states (e.g., optical properties and photoemission behavior). Qualitatively, the most striking effects will be the introduction of anisotropy, corresponding to the departure from cubic symmetry, into various properties. For example, the diagonal elements of the dielectric constant tensor, giving the optical absorption, no longer will be equal. Also, for cubic magnetic metals,

such as Ni, a magnetocrystalline anisotropy of lower order than the usual fourth-order cubic term will appear. For some years the existence of such a "surface magnetic anisotropy" has been discussed and invoked on various occasions to justify certain experimental behavior.[1] Indeed, much of the original motivation in undertaking the present investigation was to make possible a realistic estimate of the importance of this "surface magnetic anisotropy" for real systems.

Our treatment follows from that of Goodwin,[2] who treated a single band within the tight-binding approximation in a simple geometrical situation. The situation Goodwin treated is equivalent to that of a single d band in a thin film crystal of fcc structure having a $\langle 100 \rangle$ direction as normal. Our aim then is to generalize Goodwin's treatment in a way that allows us to treat the electronic structure of thin films of transition and noble metals. Those materials involve more than one d band, and exhibit geometrical complications.

The single-band tight-binding problem involves solving a single second-order difference equation plus the pertinent boundary conditions. For many bands (five in the full d-band problem, two if one treats only the Γ_{12} bands as we do in our examples below), one has a set, equal to the number of bands, of coupled second-order difference equations. (It is the assumption of having only nearest-neighbor overlap integrals that restricts the order of the difference equations to second order for $\langle 100 \rangle$ and $\langle 111 \rangle$ films. Even with this assumption, the equations for films with other normals in general will be higher order.) In the case where a layer of the film is a mirror plane of the crystal (such as a fcc film with a $\langle 100 \rangle$ direction as normal), as shown below, this extension to a set of coupled difference equations does not offer any fundamental difficulty. Formally, this relative simplicity arises from the fact that the coefficients in the difference equations are all real. However, in the case where a layer of the crystal is not a plane of reflection symmetry (such as for a fcc film with a $\langle 111 \rangle$ direction as normal), in general the coefficients in the difference equations are complex. For a single band, one can remove this difficulty by performing operations that amount to factoring out a common phase factor.[3] However, for more than one band, this phase factor differs from band to band, and the solution of the eigenvalue problem for the set of coupled difference equations plus coupled boundary equations is quite complicated. We have, however, successfully solved this problem using numerical techniques.

Our basic results can be roughly categorized as size effects and surface effects. By size effects we mean those changes in behavior of the energy eigenvalues and eigenstates from the bulk band behavior in the situation where one terminates the crystal at sharply defined boundaries without changing the values of overlap integrals, either within the boundary planes or within the interior of the film, from the bulk values. Such effects occur because of the loss of translational and cubic symmetry in a thin crystal. By surface effects, we mean changes in behavior associated with changes in the values of overlap integrals, within the boundary planes.

We find that to each energy eigenvalue of a film there correspond values of an angular variable θ that itself corresponds to the product of the wave vector times the lattice parameter (ka) in the bulk limit. For the single-band situation for both $\langle 100 \rangle$ and $\langle 111 \rangle$ films, in the absence of surface effects each energy eigenvalue corresponds to a single value of the magnitude of θ. Making the correspondence between θ and ka (with the appropriate phase shift in the $\langle 111 \rangle$ case), we see that for a crystal of N layers the N energy eigenvalues lie on top of the corresponding bulk band ($\vec{k}$ parallel to the film normal) and are equally spaced in θ. For a $\langle 100 \rangle$ film with two or more interacting bands, this remains true. However, for a $\langle 111 \rangle$ film with two or more interacting bands, the situation changes. In the absence of surface states, the film energy eigenvalues continue to fall on top of the bulk bands, but they are no longer evenly spaced in θ, and in general more than one value of θ corresponds to a given energy. (Thus, one might expect any difference between bulk and film density of states to be greater for $\langle 111 \rangle$ films.)

For the single-band case,[2] when the overlap integrals within the surface layers depart from their values for planes within the interior of the film, the distribution of energy eigenvalues versus angular variable θ changes. For a large enough difference in the overlap integrals, two of the states no longer lie on the bulk band. These states are surface states, i.e., their charge density decays exponentially on going into the crystal. We have examined and described below the corresponding behavior for two interacting d bands in a $\langle 100 \rangle$ crystal. (For a real noble or transition metal, the d-band surface states are, of course, degenerate with conduction-band states. Interaction effects then lead us to expect the surface states to be virtual states. There may, however, still be appreciable effects on the density of states; especially since surface states can be a greater proportion of the total number of states for a thin film than for a bulk crystal.)

A particularly striking qualitative feature of the

⟨111⟩ film behavior is the appearance of certain "intrinsic" surface states, even when the overlap integrals within the boundary planes are the same as those within planes in the interior of the film.

In our numerical illustrations of both the size and surface effects, we treat the case of two d bands corresponding to the Γ_{12} bands in nonmagnetic Ni. [Rather than using Fletcher's *a priori* calculated values[4] of the pertinent overlap integrals, we use the values determined by Hodges *et al.*[5] in their parametrization scheme based on Hanus's[6] augmented-plane-wave (APW) calculated bands for nonmagnetic Ni.]

In Sec. II we discuss the formal analysis of the size effect on the d electron states. We begin by summarizing the previous results for the single-band case, and then go on to treat two interacting bands both for the case where the coupling coefficients in the difference equations are real and for the case where they are complex. (The extension to more than two bands will be obvious.) In Sec. III, we discuss the analysis necessary to treat the surface effects, i.e., change of overlap integrals within the surface planes and the consequent appearance of surface states, for a ⟨100⟩ film. In Sec. IV we present typical size effects exhibited by the Γ_{12} d bands in ⟨100⟩ and ⟨111⟩ film crystals. In that section, we also show examples of the development of surface states for a ⟨100⟩ film with changing surface overlap integrals. In addition to these usual surface states, we illustrate the existence of the intrinsic surface states for ⟨111⟩ films. Finally, we discuss some possibilities for experimentally observing significant physical manifestations of the effects of size and surface on the d-band electronic structure.

II. ANALYSIS OF SIZE EFFECTS ON d-BAND STRUCTURE

A. Review of Single-Band Behavior

We begin by reviewing the previous results[2,3] for the size effect on a single band (i.e., an s-like band) in the tight-binding approximation for a cubic lattice. We consider a slablike single-crystal sample having N atomic layers, where N is a rather small integer, say 5 or 10. Each of these layers in turn is infinite in its two dimensions. We then treat each of the layers as a periodic two-dimensional crystal (i.e., we apply the usual Bloch treatment, but in two rather than three dimensions). Our fundamental assumption is to seek wave functions for the film sample that are linear combinations of the Bloch wave functions that hold for the individual layers. This viewpoint is that of the tight-binding approximation, and we also treat the layer wave functions in that approximation.

1. *Real Coupling Coefficients (Reflection Symmetry in Plane of Film)*

The wave functions for the film are

$$\Psi_{p_2p_3}=\sum_{l=1}^{N} S_l\psi^l_{p_2p_3} \quad , \tag{2.1}$$

where

$$\psi^l_{p_2p_3}=\frac{1}{(N_2N_3)^{1/2}}\sum_{m=1}^{N_2}\sum_{n=1}^{N_3} \times\left[\exp i\left(2\pi\frac{p_2}{N_2}m+2\pi\frac{p_3}{N_3}n\right)\right]\varphi(\vec{r}-\vec{r}_{lmn}) \tag{2.2}$$

is the tight-binding wave function for the lth layer. Here $\varphi(\vec{r}-\vec{r}_{lmn})$ is the atomic wave function centered on the lattice point $\vec{r}_{lmn}$. A two-dimensional Brillouin zone may be defined for each layer. (The form of this zone will be discussed below in Sec. IV for the cases where the layers are ⟨100⟩ or ⟨111⟩ planes of the crystal.) Here p_2/N_2 and p_3/N_3 (with p_2 and p_3 integers $\leq N_2$ and N_3, respectively) label a point in that zone. Since there is translational symmetry in two dimensions, p_2/N_2 and p_3/N_3 are good quantum numbers and serve to label the three-dimensional wave function given in (2.1).

For each point in the two-dimensional Brillouin zone, there are N discrete quantized states of the form given in (2.1). As the number of layers N becomes large, these N states simply map out the energy band corresponding to wave vector normal to the layers.

The condition that $\Psi_{p_2p_3}$ satisfies Schrödinger's equation gives

$$\langle\psi^l_{p_2p_3}\,|\,\mathcal{H}-E\,|\,\Psi_{p_2p_3}\rangle=0 \quad . \tag{2.3}$$

The use of only nearest-neighbor overlap integrals in (2.3) leads to the second-order difference equation for S,

$$0=RS_{l+1}+(F-E)S_l+RS_{l-1}, \quad 2\leq l\leq N-1 \ . \tag{2.4}$$

This equation with real coefficients holds in a case where there is reflection symmetry, e.g., a ⟨100⟩ crystal for the fcc lattice. For such a ⟨100⟩ fcc crystal,

$$\langle 100\rangle, \quad F=2A\left[\cos\left(\frac{2\pi p_2}{N_2}\right)+\cos\left(\frac{2\pi p_3}{N_3}\right)\right]+E_0+\Delta \ , \tag{2.5}$$

$$A=\int\varphi^*(\vec{r}-\vec{r}_{\text{near neigh.}})(V-U)\varphi(\vec{r})d^3r \tag{2.6}$$

is the nearest-neighbor overlap integral (defined for a lattice site at the origin). (Here, as usual, $V-U$ is the difference between the crystal potential and that of an isolated atom.) In practice, we treat all overlap integrals as adjustable parameters, and in our numerical examples adopt currently accepted values.[5] The same is true of the

single center energy E_0 and the crystal-field splitting Δ. The coefficient giving the interaction between adjacent planes is

$$\langle 100\rangle, \quad R = 2A\left[\cos\left(\frac{\pi p_2}{N_2}+\frac{\pi p_3}{N_3}\right)+\cos\left(\frac{\pi p_2}{N_2}-\frac{\pi p_3}{N_3}\right)\right] . \tag{2.7}$$

If the overlap integrals do not change within the boundary planes,

$$O = RS_2 + (F-E)S_1 \quad , \tag{2.8a}$$

$$O = (F-E)S_N + RS_{N-1} \quad . \tag{2.8b}$$

Equation (2.4) is a second-order difference equation with boundary conditions given by (2.8). We seek a general solution of (2.4) of the form

$$S_l = \beta^l \quad . \tag{2.9}$$

The particular solutions corresponding to eigenvalues of E are then the linear combinations of such solutions necessary to satisfy (2.8).

With the substitution (2.9), Eq. (2.4) becomes

$$O = R\beta^2 + (F-E)\beta + R \quad . \tag{2.10}$$

Thus the bulk equation (2.4) gives a quadratic equation in β for specified E. (This equation is analogous to a dispersion relationship between energy and wave number for Bloch waves.)

We note that if β_1 is a root of (2.10), then $1/\beta_1$ is also a root. Since β_1 and $1/\beta_1$ are roots of a real quadratic, they are either both real or are complex conjugates. Then β_1 is either a complex number of modulus unity, or β_1 is real. The real solutions for β correspond to surface states which we shall consider in Sec. III. In the present case (where overlap integrals are the same within bulk and surface planes) we seek solutions of the form

$$\beta = e^{i\theta} \quad , \tag{2.11}$$

so that $$E = F + 2R\cos\theta \quad . \tag{2.12}$$

For E, and hence θ, to be an eigenvalue, the solution given by (2.11) and (2.12) must also satisfy (2.8). Since the energies for $+\theta$ and $-\theta$ are degenerate, we seek eigenfunctions of the form

$$S_l = ae^{il\theta} + be^{-il\theta} \quad . \tag{2.13}$$

From (2.8a), substituting (2.12) for E, we have

$$b = -a \quad , \tag{2.14a}$$

and thus $$S_l = \sin l\theta \quad . \tag{2.14b}$$

To satisfy (2.8b) with S_l given by (2.14b) in turn requires that

$$O = \sin(N+1)\theta \quad . \tag{2.15}$$

This gives the eigenvalues of θ,

$$\theta = \theta_m = \frac{m\pi}{(N+1)} , \quad m = 1, 2, \ldots, N \tag{2.16}$$

and the eigenvalues of E are given by (2.12) for these values of θ. In a plot of E versus θ, the eigenvalues are then evenly spaced along the θ axis between $\pi/(N+1)$ and $N\pi/(N+1)$. We note that the eigenfunctions have well-defined parity with respect to the central plane of the film. The parity is even for odd m, and odd for even m. Actually, the parity property of the equation with real coefficients (corresponding to reflection symmetry through the central plane of the film) means that rather than using the $l = N$ boundary condition, one can find all eigenfunctions by using only the $l = 1$ boundary condition and specifying the parity.

2. *Complex Coupling Coefficients (No Reflection Symmetry in Plane of Film)*

In the case of a $\langle 111\rangle$ film of an fcc lattice, there is no longer mirror symmetry through the center plane of the film, and instead of (2.4) and (2.8) we have

$$O = R^*S_{l+1} + (F-E)S_l + RS_{l-1}, \quad 2 \le l \le N-1 \tag{2.17}$$

$$O = R^*S_2 + (F-E)S_1 \quad , \tag{2.18a}$$

$$O = (F-E)S_N + RS_{N-1} \quad , \tag{2.18b}$$

where $$R = re^{-i\delta} \tag{2.19}$$

is a complex number. For a single S-like band in a $\langle 111\rangle$ fcc film,

$$\langle 111\rangle, \quad F = 2A\left[\cos\left(\frac{2\pi p_2}{N_2}\right)+\cos\left(\frac{2\pi p_3}{N_3}\right)+\cos\left(\frac{2\pi p_2}{N_2}-\frac{2\pi p_3}{N_3}\right)\right]+E_0+\Delta \quad , \tag{2.20}$$

$$\langle 111\rangle, \quad R = A\left\{\exp\left[\frac{i}{3}\left(\frac{-4\pi p_2}{N_2}+\frac{2\pi p_3}{N_3}\right)\right]+\exp\left[\frac{i}{3}\left(\frac{2\pi p_2}{N_2}+\frac{2\pi p_3}{N_3}\right)\right]+\exp\left[\frac{i}{3}\left(\frac{2\pi p_2}{N_2}-\frac{4\pi p_3}{N_3}\right)\right]\right\} . \tag{2.21}$$

We seek[3] a general solution of (2.17) of the form

$$S_l = \beta^l = (e^{-i\delta}\gamma)^l \quad . \tag{2.22}$$

This form allows us to factor out $e^{-il\delta}$ in (2.17), and obtain

$$0 = r\gamma^2 + (F-E)\gamma + r \quad . \tag{2.23}$$

Thus, for the single band, the relationship between E and γ remains the same as that between E and β in the real coefficient case when R is replaced by its modulus. With

$$\gamma = e^{i\theta} \quad , \tag{2.24}$$

$$E = F + 2r\cos\theta \quad , \tag{2.25}$$

and to satisfy the boundary equations (2.18), the eigenvalues of θ, and hence E, are again given by (2.16). We note, however, that because of the factor $e^{-i\delta}$ in (2.22), the eigenfunctions no longer have well-defined parity.

B. Two Bands with Real Coupling Coefficients (⟨100⟩ Film)

For more than one band (2.1) is replaced by

$$\Psi_{p_2 p_3} = \sum_{j=1}^{n_d} \sum_{l=1}^{N} S_{jl} \psi^{l}_{j p_2 p_3} \quad , \tag{2.26}$$

where j is summed over the number of d bands present ($n_d = 5$ in the full d-band problem, and $n_d = 2$ in our two-band Γ_{12} examples), and

$$\psi^{l}_{j p_2 p_3} = \frac{1}{(N_2 N_3)^{1/2}} \sum_{m=1}^{N_2} \sum_{n=1}^{N_3} \times \left[\exp i\left(2\pi \frac{p_2}{N_2} m + 2\pi \frac{p_3}{N_3} n\right)\right] \varphi_j(\vec{r} - \vec{r}_{lmn}) \tag{2.27}$$

is the tight-binding basis wave function for the lth layer corresponding to the jth atomic d wave function.

For the case of two coupled bands (e.g., the Γ_{12} d bands, corresponding to the E-symmetry atomic d states, in the fcc lattice) (2.17) is replaced by two coupled second-order difference equations. For $2 \leq l \leq N-1$,

$$O = R^*_{11} S_{1l+1} + (F_1 - E) S_{1l} + R_{11} S_{1l-1} + R^*_{12} S_{2l+1} + J_{12} S_{2l} + R_{12} S_{2l-1} \quad , \tag{2.28a}$$

$$O = R^*_{12} S_{1l+1} + J_{12} S_{1l} + R_{12} S_{1l-1} + R^*_{22} S_{2l+1} + (F_2 - E) S_{2l} + R_{22} S_{2l-1} \quad . \tag{2.28b}$$

We shall give the specific form of the various coefficients in Sec. IV below. The $l = 1$ boundary equations are

$$O = R^*_{11} S_{12} + (F_1 - E) S_{11} + R^*_{12} S_{22} + J_{12} S_{21} \quad , \tag{2.29a}$$

$$O = R^*_{12} S_{12} + J_{12} S_{11} + R^*_{22} S_{22} + (F_2 - E) S_{21} \quad . \tag{2.29b}$$

In this section, we treat the case where the coefficients R_{ij} in (2.28) and (2.29) are real. This applies to the situation where a layer of the film is a mirror plane of the crystal (e.g., a film with a ⟨100⟩ direction as normal for an fcc lattice). Since in that case parity is a good quantum number, if we satisfy the $l = 1$ boundary conditions for functions of specified parity, we will satisfy the $l = N$ boundary conditions.

We can view (2.28) as a vector equation

$$\mathcal{O} \begin{pmatrix} S_{1l-1} \\ S_{2l-1} \end{pmatrix} = 0 \quad , \tag{2.30}$$

with $$\mathcal{O} = \begin{bmatrix} O_1 & O_3 \\ O_3 & O_2 \end{bmatrix} \quad , \tag{2.31}$$

and taking the R_{ij} as real,

$$O_1 = R_{11}\omega^2 + (F_1 - E)\omega + R_{11} \quad , \tag{2.32a}$$

$$O_2 = R_{22}\omega^2 + (F_2 - E)\omega + R_{22} \quad , \tag{2.32b}$$

$$O_3 = R_{12}\omega^2 + J_{12}\omega + R_{12} \quad . \tag{2.32c}$$

Here ω is the translation operator,

$$\omega S_l = S_{l+1} \quad . \tag{2.33}$$

Similarly, we can represent (2.29) as

$$\mathcal{P} \begin{pmatrix} S_{11} \\ S_{21} \end{pmatrix} = 0 \quad , \tag{2.34a}$$

with $$\mathcal{P} = \begin{bmatrix} P_1 & P_3 \\ P_3 & P_2 \end{bmatrix} \tag{2.34b}$$

and $$P_1 = R_{11}\omega + (F_1 - E) \quad , \tag{2.35a}$$

$$P_2 = R_{22}\omega + (F_2 - E) \quad , \tag{2.35b}$$

$$P_3 = R_{12}\omega + J_{12} \quad . \tag{2.35c}$$

Let us designate T^m_l as the mth eigenfunction of the two single noninteracting bands [i.e., the bands with $R_{12} = 0$, $J_{12} = 0$, given by (2.14) and (2.16)]. We shall now show that the eigenfunctions of the interacting two-band problem are given by

$$\begin{pmatrix} S_{1l} \\ S_{2l} \end{pmatrix} = \underline{T}^m_l = \begin{pmatrix} a & T^m_l \\ b & T^m_l \end{pmatrix} \quad , \tag{2.36}$$

where to maintain normalization $a^2 + b^2 = 1$. In other words, we will demonstrate that θ is a good quantum number of the two-band problem with real coupling coefficients. In (2.36), the states

$$\begin{pmatrix} T^m_l \\ 0 \end{pmatrix} \text{ and } \begin{pmatrix} 0 \\ T^m_l \end{pmatrix}$$

correspond to complete occupation of the eigenstate for one or the other of the two original noninteracting bands. If a and b in (2.36) are both nonzero, then a^2 and b^2 represent the admixture of the original band-1 and band-2 states, respectively, to form the final eigenfunction of the interacting system.

We now demonstrate that the $\underline{T}^m_l$ of (2.36) are eigenfunctions of the system described by (2.28) and (2.29). In so doing, we will find the energy eigenvalues. To be an eigenfunction, $\underline{T}^m_l$ must simultaneously satisfy the condition

$$\mathcal{O} \begin{pmatrix} a\, T^m_{l-1} \\ b\, T^m_{l-1} \end{pmatrix} = 0 \tag{2.37a}$$

and $$\mathcal{P} \begin{pmatrix} a\, T^m_1 \\ b\, T^m_1 \end{pmatrix} = 0 \quad . \tag{2.37b}$$

From (2.14), (2.16), and (2.32),

$$O_1 T^m_{l-1} = \frac{1}{2i}\left[\left(\exp\frac{im\pi}{N+1}\right)^{l-1} - \exp\frac{-i2m\pi}{N+1}\left(\exp\frac{-im\pi}{N+1}\right)^{l-1}\right]\left(R_{11}\exp\frac{i2m\pi}{N+1} + (F_1 - E)\exp\frac{im\pi}{N+1} + R_{11}\right), \quad (2.38)$$

$$O_2 T^m_{l-1} = \frac{1}{2i}\left[\left(\exp\frac{im\pi}{N+1}\right)^{l-1} - \exp\frac{-i2m\pi}{N+1}\left(\exp\frac{-im\pi}{N+1}\right)^{l-1}\right]\left(R_{22} + (F_2 - E)\exp\frac{im\pi}{N+1} + R_{22}\exp\frac{i2m\pi}{N+1}\right), \quad (2.39)$$

$$O_3 T^m_{l-1} = \frac{1}{2i}\left[\left(\exp\frac{im\pi}{N+1}\right)^{l-1} - \exp\frac{-i2m\pi}{N+1}\left(\exp\frac{-im\pi}{N+1}\right)^{l-1}\right]\left(R_{12}\exp\frac{i2mn}{N+1} + J_{12}\exp\frac{im\pi}{N+1} + R_{12}\right). \quad (2.40)$$

Then substituting into (2.37a) and canceling the common first factor in (2.38), (2.39), and (2.40) we obtain

$$a\left(R_{11}\exp\frac{i2m\pi}{N+1} + (F_1 - E)\exp\frac{im\pi}{N+1} + R_{11}\right) + b\left(R_{12}\exp\frac{i2m\pi}{N+1} + J_{12}\exp\frac{im\pi}{N+1} + R_{12}\right) = 0, \quad (2.41a)$$

$$a\left(R_{12}\exp\frac{i2m\pi}{N+1} + J_{12}\exp\frac{im\pi}{N+1} + R_{12}\right) + b\left(R_{22}\exp\frac{i2m\pi}{N+1} + (F_2 - E)\exp\frac{im\pi}{N+1} + R_{22}\right) = 0. \quad (2.41b)$$

The simultaneous solution of Eqs. (2.41) requires that the 2×2 determinant of the coefficients vanish. This condition yields the two values of E corresponding to the two interacting bands.

$$E^m_{1,2} = \tfrac{1}{2}\left[F_1 + F_2 + 2(R_{11} + R_{22})\cos\left(\frac{m\pi}{N+1}\right)\right] \pm \tfrac{1}{2}\left\{\left[F_1 - F_2 + 2(R_{11} - R_{22})\cos\left(\frac{m\pi}{N+1}\right)\right]^2 + 4\left[J_{12} + 2R_{12}\cos\left(\frac{m\pi}{N+1}\right)\right]^2\right\}^{1/2}. \quad (2.42)$$

A similar calculation shows that the existence of a solution to (2.37b) requires the vanishing of the same 2×2 determinant as that given by the coefficients of (2.41). Thus $E^m_{1,2}$ of (2.42) gives the energy eigenvalues for two interacting bands with real coupling coefficients.

C. Two Bands with Complex Coupling Coefficients (⟨111⟩ Film)

In the case of a ⟨111⟩ film crystal (no reflection symmetry through central plane), the coupling coefficients between planes R_{ij} are complex:

$$R_{11} \equiv r_1 e^{-i\delta_1}, \quad (2.43a)$$

$$R_{22} \equiv r_2 e^{-i\delta_2}, \quad (2.43b)$$

$$R_{12} \equiv r_3 e^{-i\delta_3}. \quad (2.43c)$$

The difference equations for interior planes and for the $l=1$ boundary plane are given by (2.28) and (2.29), respectively. Since parity is no longer a good quantum number, we also need the $l=N$ boundary condition:

$$O = (F_1 - E)S_{1N} + R_{11}S_{1N-1} + J_{12}S_{2N} + R_{12}S_{2N-1}, \quad (2.44a)$$

$$O = J_{12}S_{1N} + R_{12}S_{1N-1} + (F_2 - E)S_{2N} + R_{22}S_{2N-1}. \quad (2.44b)$$

A calculational procedure for finding the energy eigenvalues similar to that of Sec. II B is unfortunately impossible since the eigenfunctions for bands 1 and 2 with $R_{12}=0$ are not the same, but differ because $\delta_1 \neq \delta_2$. (The difficulty is compounded by the presence of the third-phase angle δ_3.) The existence of the nonzero phases δ_1, δ_2, and δ_3 in general prevents the existence of a common factor in the equations equivalent to (2.38)–(2.40), and this in turn prevents obtaining a simple 2×2 set of equations as in (2.41).

Thus when the coupling coefficients are complex (i.e., when there is no reflection symmetry in the central plane of the crystal), θ is not a good quantum number. The solution of the eigenvalue problem for the coupled difference equations then becomes much more involved, and we have resorted to numerical calculation in this case. We here describe the numerical techniques (used for the ⟨111⟩ case as discussed in Sec. IV and also used to study surface effects in the ⟨100⟩ case as discussed in Sec. III and IV).

Equations (2.28) can be reduced to two identical uncoupled fourth-order equations for S_{1l-1} and S_{2l-1}, respectively.

$$O = \{[R^*_{11}\omega^2 + (F_1 - E)\omega + R_{11}][R^*_{22}\omega^2 + (F_2 - E)\omega + R_{22}] - [R^*_{12}\omega^2 + J_{12}\omega + R_{12}]^2\}S_{1l-1}, \quad (2.45)$$

where ω is the translation operator defined in (2.33). Then for specified E, we seek solutions for S_{1l} of the form

$$S_{1l} = \beta^l. \quad (2.46)$$

The β's are then the roots of the quartic,

$$O = [R^*_{11}\beta^2 + (F_1 - E)\beta + R_{11}][R^*_{22}\beta^2 + (F_2 - E)\beta + R_{22}] - [R^*_{12}\beta^2 + J_{12}\beta + R_{12}]^2. \quad (2.47)$$

Thus for each energy, there are four values of β. [We note from the form of (2.47) that if β_1 is a root, $1/\beta^*_1$ is also a root.] Thus the general solu-

tion for S_1 at specified E is

$$S_{1l}=\sum_{i=1}^{4} a_i \beta_i^l \quad , \tag{2.48a}$$

and the solution for S_2 is

$$S_2=\sum_{i=1}^{4} b_i \beta_i^l \quad , \tag{2.48b}$$

where the β_1 are the four roots of (2.53). In particular, in order for E to be an eigenvalue, Eqs. (2.48) must satisfy the boundary conditions (2.29) and (2.44). This gives the following 4×4 set of equations :

$$O=\sum_{i=1}^{4} a_i\left[R_{11}^{*}\beta_i^2+(F_1-E)\beta_i-(R_{12}^{*}\beta_i^2+J_{12}\beta_i)\times\left(\frac{R_{12}^{*}\beta_i^2+J_{12}\beta_i+R_{12}}{R_{22}^{*}\beta_i^2+(F_2-E)\beta_i+R_{22}}\right)\right] \quad , \tag{2.49a}$$

$$O=\sum_{i=1}^{4} a_i\left[R_{12}^{*}\beta_i^2+J_{12}\beta_i-[R_{22}^{*}\beta_i^2+(F_2-E)\beta_i]\times\left(\frac{R_{12}^{*}\beta_i^2+J_{12}\beta_i+R_{12}}{R_{22}^{*}\beta_i^2+(F_2-E)\beta_i+R_{22}}\right)\right] \quad , \tag{2.49b}$$

$$O=\sum_{i=1}^{4} a_i\left[(F_1-E)\beta_i^N+R_{11}\beta_i^{(N-1)}-(J_{12}\beta_i^N+R_{12}\beta_i^{(N-1)})\left(\frac{R_{12}^{*}\beta_i^2+J_{12}\beta_i+R_{12}}{R_{22}^{*}\beta_i^2+(F_2-E)\beta_i+R_{22}}\right)\right] \quad , \tag{2.49c}$$

$$O=\sum_{i=1}^{4} a_i\left[J_{12}\beta_i^N+R_{12}\beta_i^{(N-1)}-[(F_2-E)\beta_i^N+R_{22}\beta_i^{(N-1)}]\left(\frac{R_{12}^{*}\beta_i^2+J_{12}\beta_i+R_{12}}{R_{22}^{*}\beta_i+(F_2-E)\beta_i+R_{22}}\right)\right] \quad . \tag{2.49d}$$

Here the b_i of (2.48) have been eliminated by use of the bulk equation (2.28b) giving the b_i's in terms of the a_i's. Thus for E to be an eigenvalue, the 4×4 determinant corresponding to (2.49) must vanish.

Our numerical procedure is as follows. We scan E, and for each E solve (2.47) for the four β_i. To do this, we use Muller's method.[7] For each E, we then see whether the determinant of (2.49) vanishes. By doing successively finer scans over E in the vicinity of eigenvalues, this technique gives very accurate solutions for the eigenvalues.

III. SURFACE EFFECTS

We now consider changes in the nature of the eigenstates associated with differences between the values of overlap integrals within the boundary planes and their values within interior planes of the film. As these differences increase, the distribution of energy eigenvalues versus the angular variable θ changes. Finally, for large enough differences in the overlap integrals, for each band two of the states no longer lie in the bulk band. These states are surface states, i.e., their charge density decays exponentially on going into the crystal. In this section we present the formalism leading to these conclusions, while in Sec. IV we present an example of the behavior encountered in practice for a ⟨100⟩ crystal. We restrict our discussion here to the case of real coupling coefficients, i.e., a ⟨100⟩ film. However, it is clear that qualitatively the behavior for a ⟨111⟩ crystal film is the same. In this section, we first review the behavior for a single band,[2] and then describe the extensions of the theory necessary to treat surface states for two interacting bands.

For a single band, the bulk equation (2.4) remains unchanged,

$$O=RS_{l+1}+(F-E)S_l+RS_{l-1}\,, \quad 2\le l\le N-1 \tag{3.1}$$

while the surface equations (2.8) become

$$O=RS_2+(G-E)S_1 \quad , \tag{3.2a}$$

$$O=(G-E)S_N+RS_{N-1} \quad . \tag{3.2b}$$

If we then seek solutions of the form

$$S_l=\beta^l \quad , \tag{3.3}$$

for (3.1) we obtain

$$O=R(\beta+1/\beta)+(F-E) \quad . \tag{3.4}$$

The general solution for S_l has the form

$$S_l=a\beta^l+b(1/\beta^l) \quad . \tag{3.5}$$

The solutions have either even or odd parity. For even parity and N odd (we will here treat only the case of odd N; the final results with regard to surface-state behavior are the same for even N)

$$a\beta+b(1/\beta)=a\beta^N+b(1/\beta^N) \tag{3.6a}$$

and $$b/a=\beta^{N+1} \quad . \tag{3.6b}$$

Then, from the $l=1$ boundary condition,

$$(G-E)=-R(\beta^2+\beta^{N-1})/(\beta+\beta^N) \quad . \tag{3.7}$$

For E to be an eigenvalue, the expression for E given in (3.7) must equal that in (3.4). This then gives the condition for the eigenvalues of β giving eigenfunctions of even parity. For even parity

$$\xi=(\beta+1/\beta)-\beta(1+\beta^{N-3})/(1+\beta^{N-1}) \quad , \tag{3.8}$$

where $$\xi=(G-F)/R \quad . \tag{3.9}$$

Now the solutions for β in (3.4) occur in either

complex-conjugate pairs of modulus unity (i.e., $e^{i\theta}$ and $e^{-i\theta}$) or as pairs of real numbers which are reciprocals (β_1 and $1/\beta_1$ with β_1 real). The former correspond to propagating waves, and the latter to surface states. For $\xi = 0$, (3.8) gives the same even-parity eigenvalues for θ as in (2.16), i.e., the odd-m values in (2.16). As ξ takes on a finite value, the eigenvalues of θ shift. In particular, the $m = 1$ solution shifts toward $\theta = 0$, and finally there is a critical value of ξ at which that θ goes to zero, and a surface state of even parity first appears. (As shown by Goodwin,[2] as ξ continues to increase there are no further states of even parity.) For positive ξ, this surface state first appears when $\beta = +1$. So the threshold for the appearance of a surface state of even parity is

$$\text{threshold,} \quad \xi_{\text{even parity}} = 1 \ . \tag{3.10}$$

(For negative ξ, the threshold where $\beta = -1$ occurs for $\xi = -1$.)

One can go through the same procedure for states of odd parity, and this gives, in place of (3.8), for odd parity,

$$\xi = (\beta + 1/\beta) - \beta(1 - \beta^{N-3})/(1 - \beta^{N-1}) \ , \tag{3.11}$$

and the threshold value of ξ for the appearance of the odd-parity surface state (again as for even parity, there is only one such state per band) is

$$\text{threshold,} \quad \xi_{\text{odd parity}} = (N+1)/(N-1) \ . \tag{3.12}$$

We see that the odd-parity threshold value of ξ is always greater than the even-parity threshold of unity, but approaches unity for large N. For the single band, the threshold value of unity for the appearance of the first surface state is independent of N (the film thickness); however, as shown in Sec. IV B, this is no longer true for two interacting bands.

For the case of two interacting bands, it is no longer possible to treat analytically the changes in the electronic behavior as the overlap integrals in the surface planes change. We therefore resort to finding numerically the variation of the energy eigenvalues and the corresponding angular arguments θ, as well as the criteria for the appearance of surface states, their energy, and decay length. Actually, once having set up the numerical technique described in Sec. II C for treating the size effect for two bands with complex coupling coefficients (i.e., the $\langle 111 \rangle$ film), it is quite simple to modify the treatment to take into account surface states. One scans energy and solves for the β's as in (2.47). (For a $\langle 100 \rangle$ film, J_{12} vanishes and the R_{ij} are real.) Then one finds whether any specified energy (and the corresponding set of β's) is an eigenvalue by seeing whether a determinant coming from the boundary conditions and quite similar to the 4×4 determinant given by (2.49) vanishes. The only change from (2.49) is that the first F_i in each equation is now replaced by a G_i [analogous to the replacement of F by G in (3.2)]. [The F_2 in the final factor in each equation remains unchanged since that factor arises from the bulk relationship between the coefficients a_i and b_i of (2.48).]

As G_1-F_1 and G_2-F_2 vary, we find threshold values where a surface state first appears for each band. As shown in Sec. IV B, this threshold can be quite different for each of two interacting bands.

IV. RESULTS AND DISCUSSION

A. Size Effects

1. $\langle 100 \rangle$ *Film*

We begin by describing the two-dimensional Brillouin zone applicable to a $\langle 100 \rangle$ plane in a fcc lattice. We then give the F_i and R_{ij} determining the electronic behavior in terms of the overlap and single-site integrals, and the crystal-field parameter applicable to a "real" fcc transition or noble metal.

The lattice vectors for the two-dimensional lattice defined by a $\langle 100 \rangle$ plane of a fcc lattice are

$$\vec{r}_{mn} = m(1, 1, 0)\tfrac{1}{2}a + n(1, -1, 0)\tfrac{1}{2}a, \tag{4.1}$$

and the corresponding two-dimensional reciprocal-lattice vectors are

$$\vec{K}_2 = (1/a)(1, 1, 0) \ , \tag{4.2a}$$

$$\vec{K}_3 = (1/a)(1, -1, 0). \tag{4.2b}$$

The resulting two-dimensional Brillouin zone is given by the dashed square in Fig. 1 which is superimposed on a $\langle 100 \rangle$ view of the three-dimensional Brillouin zone.

The $\vec{k}$ vectors within the two-dimensional zone are given by

$$\vec{k} = k_2(1, 1, 0) + k_3(1, -1, 0), \tag{4.3}$$

$$\text{with} \quad k_2 = (2\pi/a)p_2/N_2 \ , \tag{4.4a}$$

$$k_3 = (2\pi/a)p_3/N_3 \ . \tag{4.4b}$$

From symmetry considerations all inequivalent $\vec{k}$'s are contained in one-eighth of the two-dimensional Brillouin zone (i.e., there are eight operations in the space group of the two-dimensional lattice) given by

$$0 \le p_2/N_2, \quad p_3/N_3 \le \tfrac{1}{2} \ . \tag{4.5}$$

When one considers only overlap integrals with nearest neighbors, for a given site in a $\langle 100 \rangle$ plane there is coupling to four sites in the same plane, to four sites in the plane above, and to four sites in the plane below. The use of a wave

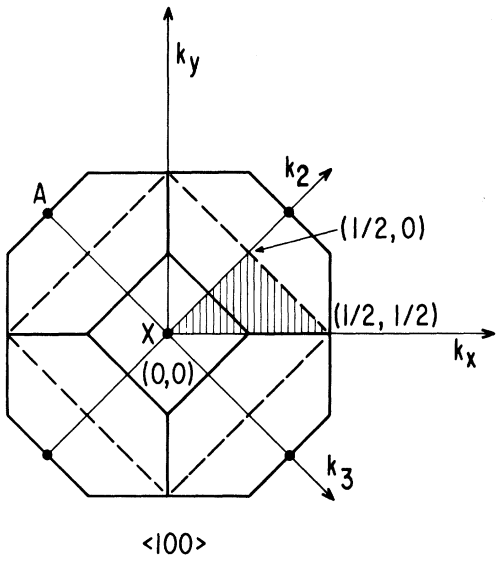

FIG. 1. Two-dimensional Brillouin zone (BZ) for ⟨100⟩ plane of fcc lattice (dashed square) superimposed on a ⟨100⟩ view of the three-dimensional BZ for a fcc lattice. All inequivalent $(p_2/N_2, p_3/N_3)$ points for the two-dimensional BZ appear in the cross-hatched triangle, the $(p_2/N_2, p_3/N_3)$ coordinates of which are indicated.

function of the form (2.26) in the Schrödinger equation as given in (2.3) determines the F_i, R_{ij}, and J_{ij} entering the difference equations (2.28) in terms of the overlap integrals A_i, single-site integral E_0, and crystal-field splitting Δ. For the Γ_{12} bands (i.e., bands corresponding to the E-symmetry atomic d states) we obtain

$$F_1 = 2(S+V)A_4 + E_0 + \Delta\,, \tag{4.6a}$$

$$F_2 = -\tfrac{2}{3}(S+V)(A_4+4A_5) + E_0 + \Delta\,, \tag{4.6b}$$

$$R_{11} = -2(X+Y)A_5\,, \tag{4.7a}$$

$$R_{22} = \tfrac{2}{3}(X+Y)(2A_4 - A_5), \tag{4.7b}$$

$$R_{12} = (2/\sqrt{3})(-X+Y)(A_4+A_5), \tag{4.7c}$$

$$J_{12} = 0\,, \tag{4.8}$$

where

$$S = \cos(2\pi p_2/N_2)\,, \tag{4.9a}$$

$$V = \cos(2\pi p_3/N_3)\,, \tag{4.9b}$$

$$X = \cos(\pi p_2/N_2 + \pi p_3/N_3)\,, \tag{4.9c}$$

$$Y = \cos(\pi p_2/N_2 - \pi p_3/N_3)\,. \tag{4.9d}$$

Here the notation for the overlap integrals follows that of Fletcher[4] and of Hodges *et al.*[5]

In all of the numerical examples we use parameter values given by Hodges *et al.*[5] for nonmagnetic Ni:

$$A_4 = 0.02091 \text{ Ry}\,, \tag{4.10a}$$

$$A_5 = 0.00413 \text{ Ry}\,, \tag{4.10b}$$

$$E_0 = 0.48392 \text{ Ry}\,, \tag{4.10c}$$

$$\Delta = -0.01301 \text{ Ry}\,. \tag{4.10d}$$

Thus, for every point in the two-dimensional Brillouin zone, one finds the film energy eigenvalues from (2.42) where the corresponding eigenvalues of θ are given by (2.16). The behavior for a typical point is shown in Fig. 2. (As shown in Sec. II, the $+\theta$ and $-\theta$ eigenvalues correspond to the same energy, so we could extend Fig. 2 out to $\theta = 360°$ by simply mirroring the figure as shown through the $\theta = 180°$ line.) As shown in Sec. II, as N varies, θ remains a good quantum number. Thus the spacing in θ between eigenvalues is constant for any N, and as N increases one simply fills in the "θ mesh." The energy eigenvalues fall on the bulk bands for $\vec{k}$ perpendicular to the plane of the film, i.e., parallel to a ⟨100⟩ direction.

For p_2, p_3 values corresponding to points within the top square face of the three-dimensional Brillouin zone (i.e., the square with center at X and corners at W), the bulk band is scanned from the p_2, p_3 point on the top face of the three-dimensional zone to the same point on the bottom face. For points outside the top square face of the three-dimensional zone, such as the $(\frac{3}{8}, \frac{1}{4})$ point studied in Fig. 2, the bulk scan consists of two segments.

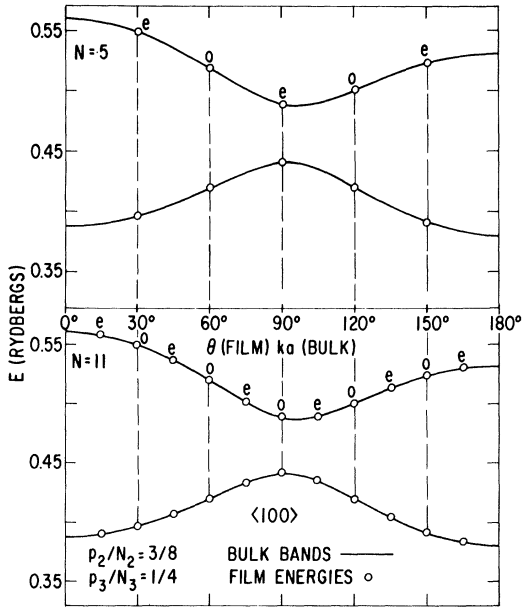

FIG. 2. Film energy eigenvalues versus θ for parameters applicable to the Γ_{12} bands in Ni with $(p_2/N_2, p_3/N_3) = (\frac{3}{8}, \frac{1}{4})$ for a ⟨100⟩ film. Parities are indicated by e (even) and o (odd). All the film energies lie on the bulk bands.

One segment scans $\vec{k}$ parallel to a ⟨100⟩ direction through the point in question, while the other segment scans $\vec{k}$ parallel to ⟨100⟩ through an equivalent point outside the two-dimensional zone but within the projection of the three-dimensional zone. For example, for the $(\frac{3}{8}, \frac{1}{4})$ point shown in Fig. 2, the scan of E versus ka between 0° and 135° corresponds to a ⟨100⟩ scan through the $(\frac{3}{8}, \frac{1}{4})$ point across the three-dimensional zone, while the scan of E versus ka between 135° and 180° corresponds to a ⟨100⟩ scan through the $(\frac{5}{8}, \frac{1}{4})$ point across the three-dimensional zone.

2. ⟨111⟩ *Film*

The lattice vectors for the two-dimensional lattice defined by a ⟨111⟩ plane of a fcc lattice are

$$\vec{r}_{mn} = m(1, -1, 0)\,\tfrac{1}{2}a + n(1, 0, -1)\tfrac{1}{2}a\,, \qquad (4.11)$$

and the corresponding two-dimensional reciprocal-lattice vectors are

$$\vec{K}_2 = (2/3a)(1, -2, 1)\,, \qquad (4.12a)$$

$$\vec{K}_3 = (2/3a)(1, 1, -2)\,. \qquad (4.12b)$$

The resulting two-dimensional Brillouin zone is given by the dashed hexagon in Fig. 3. This lies outside the ⟨111⟩ hexagonal face (solid hexagon in Fig. 3) centered at the point L of the Brillouin zone for the fcc lattice. Then the $\vec{k}$ vectors within the two-dimensional zone are given by

$$\vec{k} = k_2 a\vec{K}_2 + k_3 a\vec{K}_3\,, \qquad (4.13)$$

with k_2 and k_3 given by (4.4). From symmetry considerations all inequivalent $\vec{k}$ are contained in

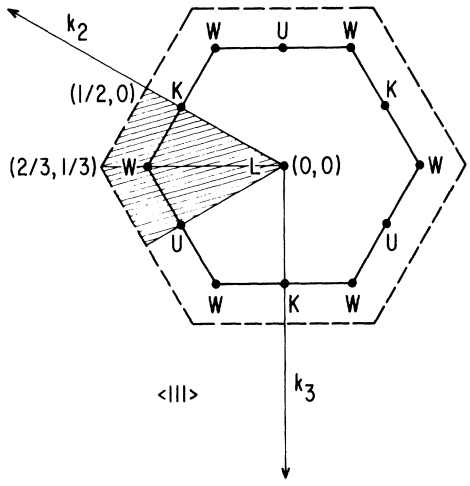

FIG. 3. Two-dimensional Brillouin zone for ⟨111⟩ plane of fcc lattice (dashed hexagon) and ⟨111⟩ face (solid hexagon) of three-dimensional BZ for fcc lattice. All inequivalent $(p_2/N_2, p_3/N_3)$ points for the two-dimensional BZ appear in the cross-hatched quadrangle.

one-sixth of the two-dimensional Brillouin zone, the cross-hatched quadrangle in Fig. 3 (i.e., there are six operations in the space group of the two-dimensional lattice). This is given by

$$0 \le p_2/N_2 \le \tfrac{1}{2}\,, \qquad (4.14a)$$

$$0 \le p_3/N_3 \le p_2/N_2\,, \qquad (4.14b)$$

for the portion to the right of the line from $(\frac{1}{2}, 0)$ through W and by

$$\tfrac{1}{2} \le p_2/N_2 \le \tfrac{2}{3}\,, \qquad (4.15a)$$

$$2p_2/N_2 - 1 \le p_3/N_3 \le 1 - p_2/N_2\,, \qquad (4.15b)$$

for the portion to the left-hand side of that line.

When one considers only overlap integrals with nearest neighbors, for a given site in a ⟨111⟩ plane there is coupling to six sites in the same plane, to three sites in the plane above, and to three sites in the plane below. Then the relationship between the coefficients of the difference equations (2.28) and the overlap integrals A_i, single-site integral E_0, and crystal-field splitting Δ follows for the Γ_{12} bands:

$$F_1 = 2SA_4 - 2(W+V)A_5 + E_0 + \Delta\,, \qquad (4.16a)$$

$$F_2 = \tfrac{2}{3}(2W + 2V - S)A_4 - \tfrac{2}{3}(W + V + 4S)A_5 + E_0 + \Delta\,, \qquad (4.16b)$$

$$R_{11} \equiv r_1 e^{i\theta_1} = TA_4 - (M+Q)A_5\,, \qquad (4.17a)$$

$$R_{22} \equiv r_2 e^{i\theta_2} = \tfrac{1}{3}(2M + 2Q - T)A_4 - \tfrac{1}{3}(M + Q + 4T)A_5\,, \qquad (4.17b)$$

$$R_{12} \equiv r_3 e^{i\theta_3} = (1/\sqrt{3})(M - Q)(A_4 + A_5)\,, \qquad (4.17c)$$

$$J_{12} = (2/\sqrt{3})(W - V)(A_4 + A_5)\,, \qquad (4.18)$$

where S and V are defined in (4.9), and

$$W = \cos(2\pi p_2/N_2 - 2\pi p_3/N_3)\,, \qquad (4.19a)$$

$$M = \exp[\tfrac{1}{3}i(2\pi p_2/N_2 + 2\pi p_3/N_3)]\,, \qquad (4.19b)$$

$$Q = \exp[\tfrac{1}{3}i(-4\pi p_2/N_2 + 2\pi p_3/N_3)]\,, \qquad (4.19c)$$

$$T = \exp[\tfrac{1}{3}i(2\pi p_2/N_2 - 4\pi p_3/N_3)]\,. \qquad (4.19d)$$

For any point in the upper triangle of the cross-hatched quadrangle in Fig. 3 [(i.e., the triangle defined by $(p_2/N_2, p_3/N_3) = (\frac{1}{2}, 0)(0, 0), (\frac{2}{3}, \frac{1}{3})$], the coefficients F_i, R_j, J_{ij} are equal to those for the corresponding point in the lower triangle mirrored across the line $p_2 = 2p_3$. Thus, to find all inequivalent energy eigenfunctions it is necessary only to consider p_2, p_3 values in the upper triangle.

Then for every point in the two-dimensional Brillouin zone, one finds the ⟨111⟩ film energy eigenvalues from (2.47) and (2.49) using the numerical procedure described at the end of Sec. II. The behavior for a typical point, $(p_2/N_2, p_3/N_3) = (\frac{1}{3}, \frac{1}{9})$, is shown in Fig. 4. In general, as N

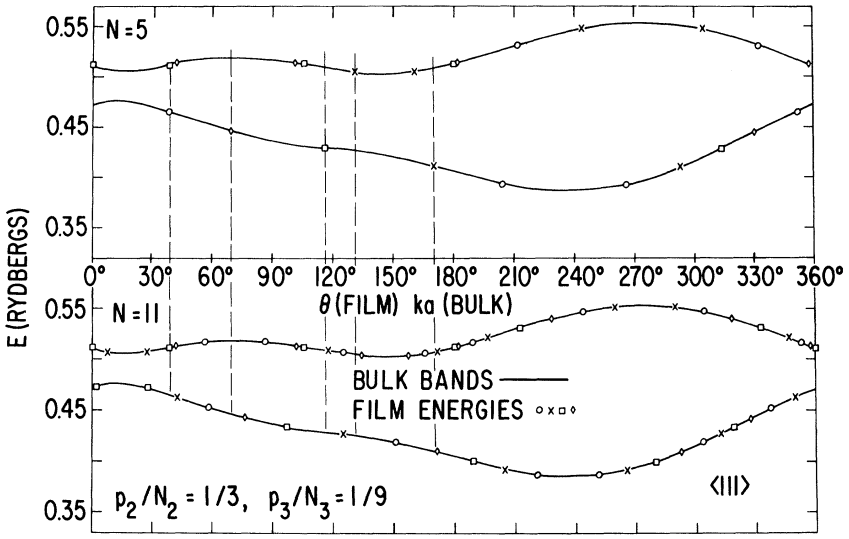

FIG. 4. Film energy eigenvalues versus θ for parameters applicable to the Γ_{12} bands in Ni with $(p_2/N_2, p_3/N_3) = (\frac{1}{3}, \frac{1}{9})$ for a ⟨111⟩ film. All the film energies lie on the bulk bands.

varies, the values of θ characterizing energy eigenvalues change. This is a consequence of the fact that when one introduces interaction between two bands for fixed N, θ is not a good quantum number; and thus the uniform spacing of energy eigenvalues versus θ, existing for the noninteracting bands, disappears. The variation with N of θ corresponding to energy eigenvalues can be seen in Fig. 4 by following a line of constant θ passing through an $N = 5$ energy eigenvalue. [Several such lines are shown in the figure. From the numerical results, in exception to the general behavior several of the energy eigenvalues and the corresponding θ are nearly, or exactly, independent of N. Since in general θ is not a good quantum number, typically several values of θ correspond to a given energy eigenfunction. To aid in quickly seeing the several values of θ for a given E, these are all represented by the same symbol in Fig. 4 (either a circle, x, square, or diamond for each E).]

The behavior for points on the line $(p_2, 0)$ is special, as illustrated in Fig. 5. The values of θ characterizing eigenvalues remain constant with increasing N. Of course, additional values of θ appear as N increases. [Since the phase angles δ_1 and δ_2 of (4.17) are not equal, the eigenvalues of θ for the upper and lower bands differ.]

For the case shown in Fig. 4, typical of $(p_2/N_2, p_3/N_3)$ values falling to the right of the line $(\frac{1}{2}, p_3/$

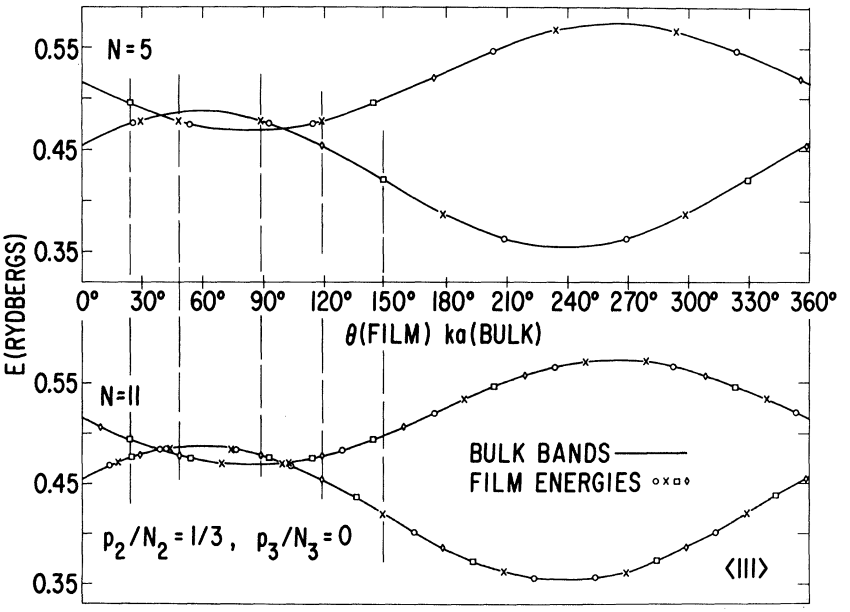

FIG. 5. Film energy eigenvalues versus θ for parameters applicable to the Γ_{12} bands in Ni with $(p_2/N_2, p_3/N_3) = (\frac{1}{3}, 0)$ for a ⟨111⟩ film. All the film energies lie on the bulk bands.

N_3) in the two-dimensional Brillouin zone of Fig. 3, all the film energies fall on the bulk bands. However, since the energy values do not fall uniformly along θ, the possibility of significant departures from the bulk density of states appears to be greater than for ⟨100⟩ films.

B. Surface Effects

1. ⟨100⟩ *Film*

Using the numerical technique described at the end of Sec. III, we have studied surface effects for the typical point $(p_2/N_2, p_3/N_3) = (\frac{3}{8}, \frac{1}{4})$. Our aim is to illustrate the qualitative effects involved, and for this purpose we adopt a crude model of the change in the overlap integrals A_i and crystal-field splitting Δ within the surface planes. We consider the case where the A_i and Δ differ from the bulk values by some scaling constant α. Then G_1 and G_2 used in the modification of (2.49) described at the end of Sec. III are given by

$$G_1 = [2(S+V)A_4 + \Delta]\alpha + E_0 \,, \qquad (4.20a)$$

$$G_2 = [-\tfrac{2}{3}(S+V)(A_4 + 4A_5) + \Delta]\alpha + E_0 \,, \qquad (4.20b)$$

with S and V given by (4.9). As already stated, in all our numerical calculations we use the values pertinent to Ni given in (4.10). Figure 6 then shows the change in behavior as α increases from unity.

For the point $(\frac{3}{8}, \frac{1}{4})$, the behavior at which is shown in Fig. 6, $R_{11} = -0.00447$ Ry, $R_{22} = 0.01360$ Ry, and $R_{12} = 0.03778$ Ry. Since R_{11} and R_{22} differ by about a factor of 3, we expect significant differences between the development of surface states in the two bands. (For $R_{12} = 0$, an even-parity surface state would occur for the lower Γ_{12} band for $\alpha = 1.105$, and for the upper band for $\alpha = 3.934$.) Since R_{12} is larger than either R_{11} or R_{22}, we expect the interaction to considerably alter the behavior from that when $R_{12} = 0$.

As α increases from unity, one rapidly sees significant effects on the lower band. For $\alpha = 1.7$, the lowest even-parity state has shifted its θ value from 150° to a value about half-way to the band edge at 180°. (Once α increases from unity, θ is no longer a good quantum number, and thus two values of θ often correspond to a single energy eigenvalue in Fig. 6.) For a value of α between 1.84 and 1.85 with $N = 5$, a surface state of even parity first appears at the lower band edge. {In contrast to the single band behavior discussed in Sec. III [see Eq. (3.10)], this threshold value of α depends on N and increases to α between 1.88 and 1.89 for $N = 11$.} For α slightly larger, an odd-parity surface state appears at the band edge at 180°. So that by $\alpha = 2.4$, as shown in Fig. 6, both surface states for the lower band have moved well below the band

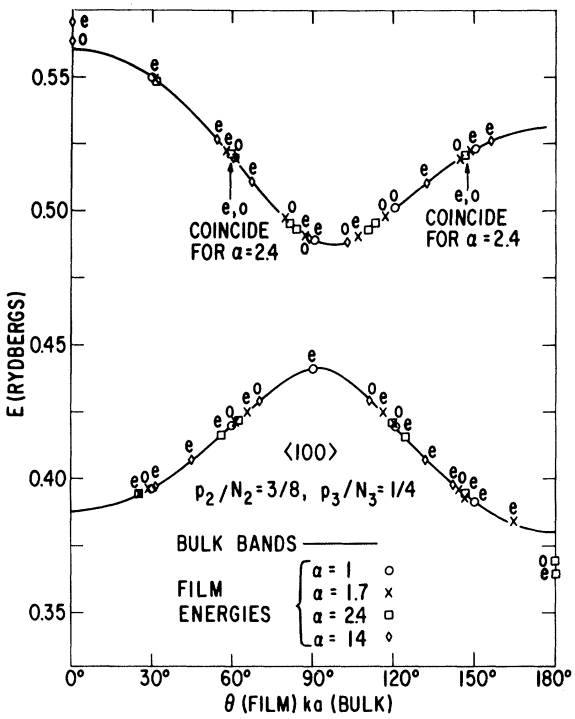

FIG. 6. Development of surface states for a ⟨100⟩ film as overlap integrals and crystal-field splitting within surface planes vary. Parity of states is indicated by e (even) or o (odd). The behavior is shown for a five-layer film (i.e., $N = 5$).

edge. Significant changes in the upper band require much larger values of α. An even-parity surface state first appears somewhere between $\alpha = 10$ and $\alpha = 12$; and by $\alpha = 14$, both an even- and an odd-parity surface state have appeared above the upper edge of the upper band. (For this value of α, the surface states for the lower band are well below the lowest energies shown in Fig. 6.)

For a real noble or transition metal, the d-band surface states are, of course, degenerate with conduction-band states. Interaction effects then lead us to expect these surface states to be virtual states. There may, however, still be appreciable effects on the density of states. Since surface states can be a greater proportion of the total number of d states for a thin film than for a bulk crystal (e.g., 40% for an $N = 5$ case), these effects can be substantial.

2. *"Intrinsic" Surface States for* ⟨111⟩ *Film*

For ⟨111⟩ films even when the overlap integrals and crystal-field effects within the surface planes are identical to those within the interior planes, surface states appear for points in the two-dimensional zone of Fig. 3 to the left of the line through the points $(p_2/N_2, p_3/N_3) = (\frac{1}{2}, 0)$ and $(\frac{1}{2}, \frac{1}{4})$, i.e., *W*

The way in which these states develop is most easily shown by following the variation in behavior along the line $p_2 = 2p_3$, for which the energy bands are symmetric about $\theta = 180°$.

Between (0, 0) and $(\frac{1}{2}, \frac{1}{4})$ (i.e., between L and W), the behavior is normal, i.e., no surface states exist. At $(\frac{1}{2}, \frac{1}{4})$ the energy gap goes to zero, and then opens up again as p_2 increases. We have followed the behavior with increasing p_2 for $N = 5$ and $N = 11$. As p_2/N_2 increases beyond $\frac{1}{2}$, intrinsic surface states first appear for $N = 11$. (At $p_2/N_2 = \frac{19}{39}$, such surface states exist for $N = 11$, but not for $N = 5$.) However, such states rapidly appear for $N = 5$. Figure 7 shows the behavior for $(\frac{5}{9}, \frac{5}{18})$ where the surface states for $N = 11$ are further into the gap than those for $N = 5$. The appearance of these intrinsic surface states may be associated with the flattening of the bands on going toward the corner of the two-dimensional Brillouin zone at $\langle \frac{2}{3}, \frac{1}{3} \rangle$.

We have also examined points off the $p_2 = 2p_3$ axis with $p_2/N_2 > \frac{1}{2}$, in particular $(\frac{5}{9}, \frac{1}{9})$ and $(\frac{5}{9}, \frac{2}{9})$, and two surface states in the gap also appear for both $N = 5$ and $N = 11$. Thus, the appearance of surface states seems to be an intrinsic property of points in the outer part of the two-dimensional Brillouin zone.

C. Possibilities for Experimental Work

Roughly speaking there are two ways in which the general effects we have been discussing could show up experimentally: in density-of-states measurements and in the appearance of anisotropy terms in various properties.

The best way to look for density-of-states effects is probably through optical or photoemission behavior. While there has been some debate in recent years as to whether or not the direct transition picture is appropriate for describing the optical properties of noble and transition metals[8,9] the weight of current evidence[10,11] seems to be in favor of the direct transition picture. The optical data can be analyzed in this picture to yield the joint density of states of the bands involved in the optical transitions. Since the size effects we have discussed involve energy shifts on the order of $1/N^2$ of the d bandwidth, any change in the d-band density of states due to size effects will be rather small. Of course, the conduction bands are much wider, and the net effect on the optical absorption may be significant.

One way to maximize the possibility of observing any net size and surface effect on the density of states would be through the use of "sandwich" films.[12] By depositing alternate thin layers of appropriate metals, one could create a situation where the d bands "see" films a few tens of atomic layers thick, while the free-electron-like bands are continuous through the whole film. Since the optical skin depth is some hundreds of atomic layers, one could have many alternating thin films within one sample. For example, alternate layers of aluminum and silver might be used. Then to a good approximation, the d bands exist only within the silver, while the conduction bands would be continuous. The importance of size and surface effects could be measured by comparing the interband optical absorption[8] for such a sandwich film to that of a continuous film with the same total thickness of silver. Another possibility would be to use alternate layers of gold (or copper) and silver. Since the d bands in Ag are about 2 eV lower[8] than in Au (or CuP, i.e., compared to a common Fermi energy, one would see reasonably well sep-

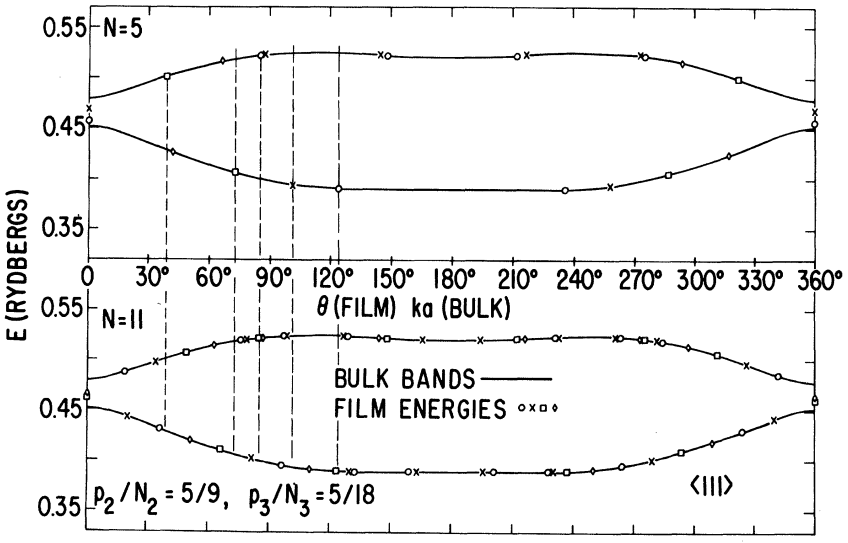

FIG. 7. Film energy eigenvalues versus θ for parameters applicable to Γ_{12} bands in Ni with $(p_2/N_2, p_3/N_3) = (\frac{5}{9}, \frac{5}{18})$ for a ⟨111⟩ film. Two states have energies in the gap, while the remaining film energies lie on the bulk bands.

arated Au and Ag interband optical absorption, and could compare the results to those for solid films of the same total thickness of one or the other material.

It is, however, difficult to be optimistic about the possibility of observing size- and surface-dependent effects on the density of states. Any simple single-layer single-crystal film will probably give a small net effect. On the other hand, the use of sandwich films, while offering the potential of enhancing the net effect, may eliminate the possibility of obtaining single crystals. For polycrystalline samples, averaging effects may tend to eliminate any significant deviation from the bulk density of states.

The possibility of observing anisotropic behavior associated with size and surface effects seems to be much more promising. Here, one could use very thin single-crystal films and look for effects simply absent for strictly cubic systems. One possibility would be to look at the optical absorption and examine the diagonal elements of the dielectric constant tensor for a departure from equality. Another possibility (and one for which we hope to pursue the theoretical analysis and to estimate the size reasonably accurately) is the appearance of a magnetocrystalline anisotropy energy of second order in the components of magnetization, as opposed to the usual fourth-order cubic anisotropy.[13] In the absence of cubic symmetry, the spin-orbit interaction viewed as a perturbation on the band energies gives a net anisotropic contribution in second rather than the usual fourth order, and thus such an effect might be appreciable. This could then be observed by torque, or more likely, ferromagnetic resonance measurements. (If one could make sandwich single-crystal films, one could obtain a very large total effect by using a Ni and Al or Ag sandwich.) Our present calculations should serve as a reasonable basis for estimating the size and nature of such effects.

ACKNOWLEDGMENTS

We are grateful to Miss E. Kreiger for her very great aid in all aspects of the numerical analysis and calculations involved in this work. We have benefited from interesting discussions with Dr. M. Blume and Dr. M. Garfinkel.

---

[1]L. Néel, Compt. Rend. 237, 1468 (1953); J. Phys. Radium 15, 225 (1954); for a review article dealing with such questions see I. S. Jacobs and C. P. Bean, in *Magnetism*, edited by G. T. Rado and H. Suhl (Academic, New York, 1963), Vol. III, Chap. 6.

[2]E. T. Goodwin, Proc. Cambridge Phil. Soc. 35, 205 (1939); 35, 221 (1939); 35, 232 (1939).

[3]L. Künne, Czech. J. Phys. B17, 894 (1967).

[4]G. C. Fletcher, Proc. Phys. Soc. (London) A65, 192 (1952).

[5]L. Hodges, H. Ehrenreich, and N. D. Lang, Phys. Rev. 152, 505 (1966); L. Hodges, Ph. D. thesis, Harvard University, 1966 (unpublished).

[6]J. G. Hanus, MIT Solid State and Molecular Theory Group Quarterly Progress Report No. 44, 29, 1962 (unpublished).

[7]D. E. Muller, *Math. Tables and Other Aids to Computation* 10, 208 (1956). We are grateful to Miss E. Kreiger for bringing Muller's technique to our attention and for adapting it to our problem.

[8]B. R. Cooper, H. Ehrenreich, and H. R. Philipp, Phys. Rev. 138, A494 (1965).

[9]C. N. Berglund and W. E. Spicer, Phys. Rev. 136, A1030 (1964); 136, A1044 (1964).

[10]G. Dresselhaus, Solid State Commun. 7, 419 (1969).

[11]J. F. Janak, D. E. Eastman, and A. R. Williams, in Symposium on Electron Density of States, Gaithersburg, Maryland, 1969 (unpbulished).

[12]The idea of using "sandwich" films as described developed out of discussion between M. Garfinkel and B. R. Cooper.

[13]H. Brooks, Phys. Rev. 58, 909 (1940).